Preliminary Design Study of a Fast-Ramping Magnet for Pre-Concept Design of an Electron-Ion Collider at Jefferson Lab

P. K. Ghoshal, *Senior Member, IEEE,* D. Chavez, R. Fair, *Senior Member, IEEE,* S. Gopinath, D. Kashy, P. McIntyre, T. Michalski, R. Rajput-Ghoshal, *Member, IEEE,* A. Sattarov

***Abstract* — The Jefferson Lab Electron Ion Collider (JLEIC) is a proposed new machine for nuclear physics research. The all new ion accelerator and collider complex will consist of two collider rings with a unique figure-of-eight layout to deliver a high degree of polarization in both beams. As part of the pre-concept design for the Ion ring, a 3-Tesla Super-Ferric dipole magnet was proposed utilizing a superconducting Cable-in-Conduit-Conductor (CICC) design to wind the coils which will be built by Texas A&M University. A first mechanical model of the winding for the 3T-SF-CICC dipole was built to validate that the winding structure provides the conductor geometry required to provide collider field homogeneity over large aperture. A rapid-cycling Booster synchrotron is required to inject 8 GeV beams to the Ion Ring. The Booster requires arc dipoles with the same field and aperture as those of the Ion Ring. Due to the design of the CICC with respect to the amount of stabilizer and the internal cooling mechanism employed, temperature rise of the coils during a quench event is much more rapid than for more conventional magnets. It is thus imperative that the magnet's stored energy is dissipated externally to the windings to avoid overheating the CICC and to provide adequate protection during a quench. This paper presents a preliminary design study, including AC effects inside the coils and associated risks with the aim of providing guidance for the design of the full protection system for such a magnet.**

***Index Terms*—JLEIC, Cable-In-Conduit-Conductor, Superferric dipole, quench protection**

I. Introduction

Modern nuclear physics has led to the development of Quantum Chromo-Dynamics (QCD), a theory describing strong interactions among quarks and leptons, and gluons as the carriers of the strong force. A polarized electron-ion collider (EIC) has long been envisioned as a gluon microscope for exploring the QCD frontier. To meet this need, Jefferson Lab (JLab) has proposed the Jefferson Lab Electron-Ion Collider (JLEIC), a high luminosity high polarization EIC based on the existing Continuous Electron Beam Accelerator Facility (CEBAF) electron SRF Linac. The original pre-concept proposal (for which the 3 T magnet was designed) was to deliver between 15 and 65 GeV center of mass energy collisions between electrons and ions. The ion accelerator and collider complex would deliver up to 100 GeV protons, or 40 GeV/nucleon ions. JLEIC will be a ring-ring collider, namely, both colliding electron and ion beams are stored in two figure-8 shaped rings as shown in Fig. 1 [1]. The JLEIC design was driven by the science program summarized in an EIC white paper [2]. Many significant design studies and accelerator R&D pursued over the years have concentrated on the following key topics- ion ring magnets, interaction region design and special magnets, e.g. the booster magnet.

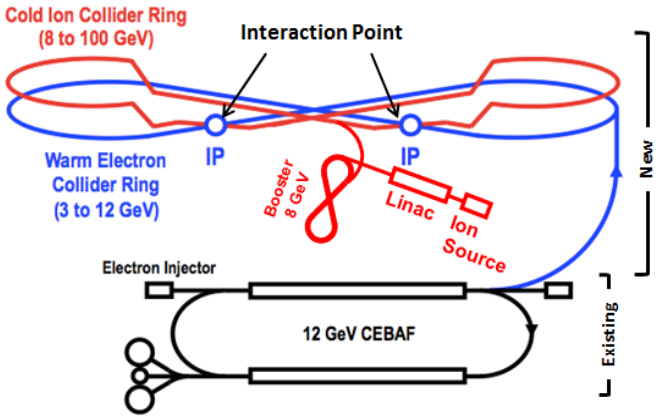

Fig. 1: A schematic drawing of the JLEIC at the JLab site

A 3T Super-Ferric (3T-SF) dipole magnet was designed by the group at Texas A&M University (TAMU), Accelerator Research Lab [3] for the requirements of the lattice of the JLEIC Ion Ring: 4 m body length, large aperture (10 x 6 cm^2) with homogeneous field, and modest ramp rate capability (0.1 T/s). The design utilizes a novel variant of superconducting Cable-in-Conduit Conductor (CICC) that provides for a particularly simple method for magnet fabrication. The cable technology and winding technology were developed and used to fabricate a first 1.2 m mechanical model of the 3T-SF-CICC dipole. Measurement of cable positions in the winding suggests that the required field homogeneity could be provided by

Manuscript receipt and acceptance dates will be inserted here.

Corresponding author: P. K. Ghoshal (e-mail: ghoshal@jlab.org)
P. K. Ghoshal, R. Fair, S. Gopinath, D. Kashy, T. Michalski, R. Rajput-Ghoshal are with the Jefferson Lab, Newport News, VA 23606 USA.
D. Chavez is with Departamento de Fisica, Universidad de Guanajuato, Leon, Gto. Mexico and Texas A&M University, Texas, TX
P. McIntyre, A. Sattarov are with Dept. of Physics & Astronomy, Texas A&M University, Texas, TX 77843 USA
Color versions of one or more of the figures in this paper are available online at http://ieeexplore.ieee.org.
Digital Object Identifier will be inserted here upon acceptance.

the CICC geometry and dipole structure. As part of the R&D activities, a prototype 1.2 m long dipole magnet is planned to be built and tested in order to evaluate its operational limits and performance parameters. This is a decisive step towards realizing production of other magnets using this NbTi-CICC technology and to guarantee stable long-term operational performance. Ion beam will be injected to the Ion Ring of JLEIC from a rapid-cycling 8 GeV Booster synchrotron. The pre-concept Booster design requires lattice dipoles of 3 T peak field, 1.2 m length, and the same aperture as that required for the arc dipoles of the Ion Ring. Thus the 3T-SF-CICC dipole design could provide an attractive option for use in the Booster ring as well. The purpose of the study reported here is to evaluate the suitability of the 3T-SF-CICC dipole design for use in the rapid-cycling Booster. Issues of AC losses, conductor stability, and quench protection are considered. Iron is presently not considered as part of the analysis reported except for the calculation of inductance.

TABLE I

SYMBOLS AND ABBREVIATIONS

t_D	Decay time (s)
μ_0	Permeability constant, $4\pi\times10^{-7}$ H/m
N_s	Number of strands [-]
d_w	Strand diameter (m)
V_{ct}	Volume of composite conductor (m^3)
T_{ch}	Charging time (s)
L_{cab}	Cable strand twist pitch (m)
L_t	Filament twist pitch (m)
B_{max}	Maximum magnetic flux density in the conductor (T)
B_{ml}	Field amplitude averaged over the winding section (T)
a_f	NbTi filament radius (m)
B_{c0}	Minimum penetration field (T)
J_c	Current density in superconductor (A/m^2)
J_{c0}	Critical current density at θ_0 and B_{c0} (A/m^2)
V_{NbTi}	Volume of superconductor (m^3)
λ	Fraction of superconductor in the composite [-]
d_{fc}	Composite filament diameter (m)
I_0	Operating current (A)
$I_C(B_{max})$	Critical current at B_{max} (A)
V_{cc}	Velocity of the fluid in the central channel (m/s)
D_{cc}	Diameter of the central channel (m)
D_h	Hydraulic diameter (m)
P	Pressure (MPa)
P_{in}	Inlet pressure (MPa)
P_{out}	Outlet pressure (MPa)
Θ	Temperature of fluid at a pressure P (K)
θ_0	Operating temperature (K)
θ_{in}	Inlet temperature at P_{in} (K)
θ_{out}	Outlet temperature at P_{out} (K)
$h_{overall}$	Overall heat transfer co-efficient ($W.m^{-2}.K^{-1}$)
$h_{overall\_UL}$	Overall heat transfer co-efficient per unit length ($W.m^{-1}.K^{-1}$)
h_{conv_SS}	Heat transfer co-efficient for flowing helium ($W.m^{-2}.K^{-1}$)
h_{cond_SS}	Heat transfer co-efficient for stainless steel tube ($W.m^{-2}.K^{-1}$)
$h_{c\_static\_He}$	Heat transfer co-efficient for static helium ($W.m^{-2}.K^{-1}$)
f_f	Friction factor, 0.045 [-]
$h_{overall\_conv}$	Overall heat transfer co-efficient ($W.m^{-2}.K^{-1}$)
ρ_{He4}	Density of helium-4 (Kg/m^3)
A_{cc}	Helium flow area in the central channel (m^2)
U	Perimeter for pressure drop (m)
Δp	Pressure drop per unit length (Pa/m)
H_{He4}	Enthalpy of Helium (J/kg)
$\dot{m}$	Mass flow rate (kg/s)
K_{He}	Thermal conductivity of helium ($W.m^{-1}.K^{-1}$)
Nu	Nusselt Number [-]
Re	Reynolds Number [-]
Pr	Prandtl Number [-]
μ_{He}	Viscosity of helium (Pa.s)
T_{cond}	Conductor temperature (K)
T_m	Maximum temperature (K)
τ	Coupling current decay time (s)
J(t)	Current density at time, t (A/m^2)
γ	Density of stabilizer (kg/m^3)
$\rho(T)$	Resistivity at temperature T (Ω.m)
C(T)	Heat capacity at T ($J.kg^{-1}K^{-1}$)
Q_{Tot}	Total heat load/loss (W)
MIITs	Quench load as 10^6.(Current)^2.time

Thus the contribution to the field due to the iron and heating effects within the iron due to fast ramping have not been evaluated. A constant heat load contribution is assumed (*due to the radiation, conduction heat from the cryogenic vessel, as well as iron losses*) to the total loss calculations. An analytical approach is adopted for the study of quench behavior of the 3T-SF booster model coil and includes AC losses (*due to eddy currents induced in electrically conductive parts*) during fast ramp up or down as well as pressure drop and heating of the coolant flow. These analyses provide a first order level of understanding of the magnet performance.

A deeper understanding of magnet behavior will be pursued at a later stage using commercially available finite element analysis codes e.g., Opera® and ANSYS®. The analytical model used (Wilson model) provides good insight into the behavior of the magnet using simple and straightforward assumptions under adiabatic conditions [4]-[6]. The symbols and abbreviations used in the paper are presented in Table I.

II. MAGNET DESIGN PARAMETERS

The SF model dipole, 3 T-1.2 m long prototype-model magnet design proposed by TAMU has two coils (top and bottom), electrically connected in series with each coil utilizing NbTi-CICC. The CICC superconducting windings are supported by a series of G11 plates & surrounded by an iron magnetic core. The basic magnet design parameters are given in Table II.

TABLE II

BOOSTER MAGNET MODEL DIPOLE COIL MAIN PARAMETERS

Parameter	**Requirement**
Magnet operating current (kA)	13.5
Magnet nominal central Field (T)	3
Magnet inductance, including iron (mH)	0.823
Peak field in the coil (T), *with iron*	3.3
Booster Magnet Field Ramp rate (T/s)	1.0
Magnetic length (m)	1.2
Beam pipe aperture (mm x mm)	100 x 60
Good field region (mm x mm)	80 x 40
Field Homogeneity (from 0.2 T to 3 T)	$<10^{-4}$
Helium Inlet temperature (K)	4.5

A. *Conductor*

The TAMU-patented [7] CICC consists of 15-strands of NbTi/Cu superconductor, wound onto a central stainless steel perforated tube. This sub-assembly is then wrapped with stainless steel foil (tape) and inserted into a Cu-Ni sheath tube which is then drawn down to compress the NbTi strands against the central tube to form the completed CICC as shown in Fig. 2.

The CICC parameters considered for the design and analysis are given in Table III. The stability of the conductor is evaluated against the design cycle of AC losses and availability of cooling power of pressurized helium flowing in the central channel of the CICC and is presented later in the following section.

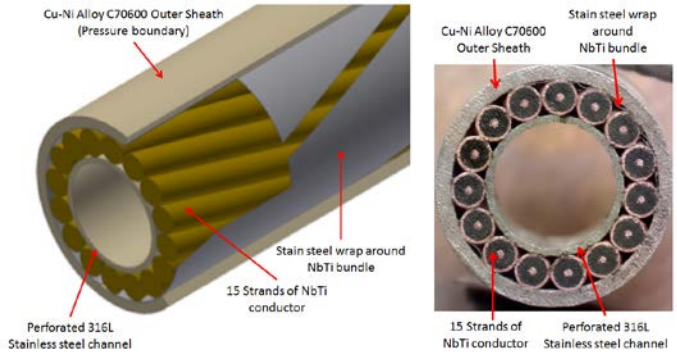

Fig. 2: A schematic and actual cross-sectional view of the TAMU CICC

TABLE III
SF MODEL DIPOLE CICC PARAMETERS

NbTi/Cu Strands	
Strand Diameter (mm)	1.2±0.0025
Ratio of Cu/Non Cu	1.5
Filament Diameter (μm)	9
# Filaments	>7400
RRR	>150
Filament twist pitch (mm)	18
I_c (A) at 6.5 T, 4.2 K (Type: VSF-SSCI-ANN)	775
Cable-In-Conduit Conductor	
# Strands	15
Strand twist pitch (mm)	76.6
Outer Tube Material	Cu-Nickel Alloy 70600
Outer Tube dia. - before drawing (mm)	9.52
Outer Tube dia. – after drawing	8.17 ± 0.02
Outer tube wall thickness (mm)	0.5
Inner Tube Material (Perforated)	316L Stainless Steel
Inner tube dia. - after drawing (mm)	4.76 ± 0.02
Inner tube wall thickness (mm)	0.25
Total conductor length for dipole (m)	85 (42.5 m per coil)

B. *Cold Mass Assembly*

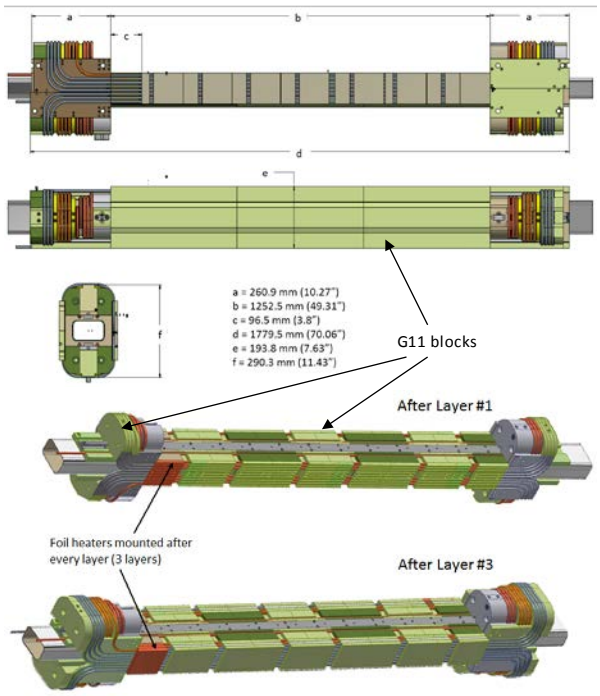

Fig. 3: Typical overall dimensions of the 1.2 m dipole showing the foil heater mounting locations after every layer.

The model SF dipole has a total of 24 turns (*12 turns per coil*), and a total cable length of about 85 m. The NbTi cable is cooled by helium flowing through the central tube. As the coolant flows through the CICC its pressure will drop. In order to avoid bubble formation the helium needs to be kept in the super-critical state throughout the winding pack. For each coil the individual coil turns are held in place using a series of G11 blocks and plates (as shown in Fig 3). A laminated iron magnetic core is fitted around the CICC winding pack. The iron core also has independent cooling tubes located within its structure. A typical model of the cold mass assembly is shown in Fig. 4.

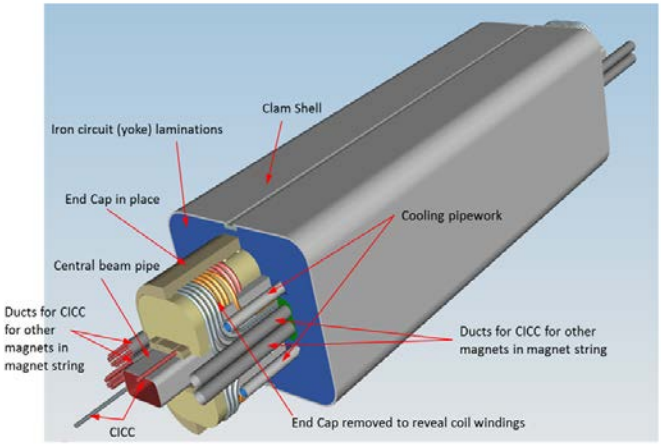

Fig. 4: A schematic of Model Dipole – Cold Mass Assembly

The main advantage of using CICC is the manufacturing/ fabrication of CICC and winding on the main support structure

for the coils are based on the design and associated bending tooling developed at TAMU. The development is envisaged to have a positive cost impact compared to a conventional Rutherford cable based on cos (nϴ) magnets.

III. SF Model Dipole Analysis

The challenges associated with this fast ramping dipole design include risks associated primarily with eddy current effects, impact on the cryogenics, magnet stability, and quench protection which were analyzed using approaches described in [4]-[6], [8]-[11]. Critical current for the conductor was established using Bottura's Model [12].

A. AC losses

Due to fast current ramping (varying field), eddy currents are induced in the conductor (wire & cable), in the iron and within the electrically conductive structural elements of the magnet. This creates AC losses under continuous operation while running the magnet up and down, based on the cycle shown in Fig 5. The losses in the CICC should be minimized by appropriate selection of conductor, while the magnet conductor cooling needs to be capable of extracting the heat loads during operation. The AC loss components are calculated based on the Wilson model [4],[5] operating at the parameters indicated in Table II [13]-[15]. The losses in the stainless steel (SS) foil and in the Copper-Nickel (CuNi) outer sheet have not been considered for the analysis here as the SS & CuNi have high electrical resistivity, and AC loss in the NbTi is considerably more prominent. In practice, the CuNi will improve the thermal capacity and stability of the conductor.

The AC loss calculations are based on a loss cycle as represented in Fig 5. The analysis presented is based on the time to reach full field, B_{max} in time t_1 as a worst case scenario. The losses are calculated for a half-cycle based on the assumption, $t_2 = t_1$ and $t_5 = t_4$ (actual time to be defined per physics requirements) making the 1-cycle period as ramp up to full field and down to zero. Therefore, the power losses are calculated based on the energy loss in a half-cycle in a given time-period (t_1 is 3 or 12 s for a ramp rate of 1 or 0.25 T/s respectively). The magnetic flux density calculated using Opera® FEA as shown in Fig 6 varies between 3.33 T and 0.02 T at an operating current of 13.5 kA, without the iron circuit (3 T at magnet center).

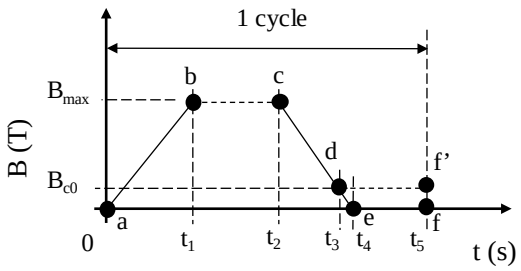

a-b: magnet ramp-up to maximum field
b-c: magnet parked at field
c-d, d-e: magnet ramp-down to a minimum or zero field
d-f': Magnet parked at a minimum field
e-f: Magnet at zero field
t_5: One cycle time period
0- t_1: Ramp up time (s)
$t_2 - t_3$ or $t_2 - t_4$: Ramp down time (s)
$t_1 - t_2$, $t_3 - t_5$ and $t_4 - t_5$: Time to be defined based on Physics requirements

Fig.5: Schematic representation of the AC loss cycle used for analysis during magnet ramping

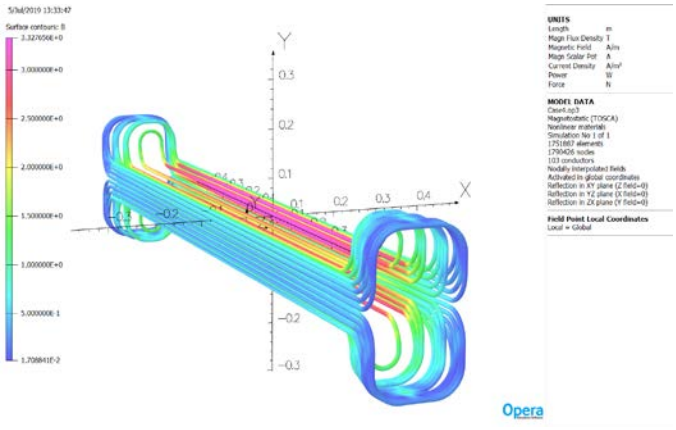

Fig. 6: Magnet field distribution over the conductor (B_{max} = 3.328 T)

The AC loss components are calculated as follows-

i. Eddy current/coupling losses (E_{EC}) – Calculated losses in the strands are the coupling losses between filaments for a half-cycle (either current ramp up or ramp down). Equation 1 suggests, τ needs to be decreased (by increasing the resistance of the material around the filament) in order to reduce the eddy current loss in the composite filamentary conductor.

$$E_{EC} = B_{ml}{}^2 \cdot \frac{8.\tau}{2\mu_0 T_{ch}} \cdot V_{ct} \cdot \left\{ 1 - \frac{\tau.\left(1 - e^{\frac{-T_{ch}}{\tau}}\right)}{T_{ch}} \right\} \quad \ldots\ldots (1)$$

The local field amplitude B_{ml} is approximated magnetic field (*flux density*) amplitude averaged over the winding section as, $B_{ml} = \frac{B_{max}}{\sqrt{3}}$.

ii. Hysteresis losses (E_{HY}) – This is calculated for a half cycle (ramp up or down). The magnetic field in the coil is ramped down to a minimum equivalent to the self-field associated with the ratio $I_0/I_C(B_{max})$ for minimum field penetration. This is to an approximation that field varies linearly over the winding and varies between minimum field penetration to maximum field, occupying an equal volume of winding.

Therefore, averaged value of hysteresis loss is calculated as (eqn. 2)-

$$E_{HY} = \frac{8}{3.\pi}.a_f.J_{c0}.B_{c0}.\left\{\frac{B_{max}+B_{c0}}{B_{max}}.\ln\left(\frac{B_{max}+B_{c0}}{B_{c0}}\right)-1\right\}.V_{NbTi} \quad .. (2)$$

Where,

$B_{c0} = B_p F_{SF}$; $F_{SF} = I_0/I_C(B_{max})$; $B_p = \mu_0 \lambda J_c \frac{d_{fc}}{2}$

iii. Penetration losses (E_P) – For a fast ramping magnet, we cannot neglect the effect of field penetration also sometimes referred to as skin effect, where current flows on the outer filaments surface and occupies a finite volume. The penetration losses in filamentary wires at B_{max} are calculated for a composite filament diameter in a fast changing longitudinal magnetic field. The losses are calculated for a half cycle (eqn. 3).

$$E_P = \frac{1}{2}\left(\frac{{B_{max}}^2}{2\mu_0}\right)\frac{4.\pi^2.\left(\frac{d_{fc}}{2}\right)^2}{{L_t}^2}Y(X)V_{NbTi} \quad .. (3)$$

Where,

$Y(X) = \frac{X}{3(1+X)^2}$ if $X < 1$; $\frac{1}{2X} - \frac{5}{12X^2}$ if $X > 1$, and $X = \frac{2\pi B_{max}}{\mu_0 \lambda J_{c0} L_t}$

iv. Self-field losses (E_{SF}) – This is associated with the loss effects due to the self-field of the wire from transport current (eqn. 4-5).

$$E_{SF} = \frac{(B_p F_{SF})^2}{2\mu_0}M(F_{SF})V_{NbTi} \quad .. (4)$$

$$M(F_{SF}) = \left[\frac{4}{F_{SF}} - 1 + \frac{4(2-F_{SF})\ln\left(\frac{2-F_{SF}}{2}\right)}{{F_{SF}}^2}\right] \quad .. (5)$$

A summary of AC losses calculated with varying ramp rates is provided in Table IV. Other external heat load has been estimated at a constant 4 W (*due to the radiation, conduction heat from the cryogenic vessel, as well as iron losses*) [16]. Detailed calculations for the radiation and iron losses shall be carried out and engineered during the design of the iron magnetic circuit and cryostat structures. The major loss components are estimated at three different ramp rates for comparison.

TABLE IV

RESULTS OF SF MODEL COIL AC LOSSES VS RAMP RATES

Loss Component	Ramp rates	1 T/s	0.5 T/s	0.25 T/s
	Charging time to reach full field	3 s	6 s	12 s
Eddy current (coupling and Magnetization) loss – filaments and strands (J)	Induced currents between SC filaments due to external field changes and between strands	79.12	39.56	19.78
Hysteretic loss (J)	Induced currents within SC filaments	8.97	8.97	8.97
Penetration loss (J)	Superconductor surface	1.77	1.77	1.77
Self-field loss (J)	Induced currents between SC filaments due to changes in the transport current	3.68	3.68	3.68
TOTAL AC LOSS, E_{Tot_ac} (J)		93.54	53.98	34.20
TOTAL AC LOSS, Q_{Tot_ac} (W) – *Only during ramp*		**31.18**	**9.00**	**2.85**
TOTAL LOSS, Q_{Tot} (W) (Includes a constant 4 W heat load)		**35.18**	**13.00**	**6.85**

Losses were recalculated with using a tighter twist pitch (7.10 mm, instead of 18 mm) which suggests that the coupling and magnetization losses in filaments and strands can be reduced by a factor of about 6 while the penetration losses increase by a factor of about 12. The AC losses are primarily dominated by magnetization losses in filaments and strands, thus the total AC loss (E_{Tot_ac}) decreases by a factor of about 2 at the higher ramp rate of 1 T/s and increases by about 10% at 0.25 T/s, as summarized in Table V.

TABLE V

SUMMARY OF AC LOSSES WITH TIGHTER FILAMENT TWIST PITCH (7.1 mm)

Loss Component	Ramp rates	1 T/s	0.5 T/s	0.25 T/s
	Charging time to reach full field	3 s	6 s	12 s
Eddy current (coupling and Magnetization) loss – filaments and strands (J)	Induced currents between SC filaments due to external field changes and between strands	12.98	6.49	3.25
Hysteretic loss (J)	Induced currents within SC filaments	8.97	8.97	8.97
Penetration loss (J)	Superconductor surface	21.38	21.38	21.38
Self-field loss (J)	Induced currents between SC filaments due to changes in the transport current	3.68	3.68	3.68
TOTAL AC LOSS, E_{Tot_ac} (J)		47.01	40.53	37.28
TOTAL AC LOSS, Q_{Tot_ac} (W) – *Only during ramp*		**15.67**	**6.76**	**3.11**
TOTAL LOSS, Q_{Tot} (W) (Includes a constant 4 W heat load)		**19.67**	**10.76**	**7.11**

B. Cooling and Temperature margin

Appropriate design of cryogenics is critical for the stable operation of the magnet. The heat load dynamics due to AC loss is based on the ramp rate, field and operating cycles per unit time. Therefore, it is critical to optimize the helium flow rate and pressure drop in the cable to allow for removal of the steady state AC losses caused by the fast ramp (1.0 T/s). A basic design temperature stability margin of 1 K for normal operation is assumed [17]. Pressure drop and temperature rise analysis are carried out to define the input pressure and flow rate limits [18]-[20]. A friction factor (f_f) of 0.045 is used for the central CICC channel throughout the analysis as measured by Chavez [21]. The pressure drop calculations are performed using the standard Darcy-Weisbach friction loss equation (and compared with the ITER conductor) [22],[23]. The helium outlet temperature is calculated based on the heat load balance over a specific length of the conductor. This estimate is primarily based on the difference between the amount of heat deposited and heat removed by Helium within the conductor.

$$\Delta p(V_{cc}, D_{cc}, P, \theta) = f_f \times \frac{1}{D_h(D_{cc})} \times \frac{\rho_{He4}(P,\theta) \times {V_{cc}}^2}{2} \quad .. (6)$$

Where, $D_h(D_{cc}) = 4 \times \frac{A_{cc}(V_{cc})}{U(D_{cc})}$; $A_{cc}(V_{cc}) = \pi.\left(\frac{{D_{cc}}^2}{4}\right)$;

and $(D_{cc}) = \pi.D_{cc}$

The Δp is calculated after every turn (using the function defined above in eqn. 6); this sets the inlet pressure for the subsequent turn and is integrated over the length in order to evaluate the overall Δp. In order to evaluate the outlet temperature of helium, a constant heat load (summarized in Table IV) distributed over the length of the conductor is used. An energy balance, utilizing the enthalpy of the flowing helium in the central channel of the CICC to extract the heat has been developed to produce stable operation. All standard thermophysical properties of helium used in the calculations have been obtained from the NIST database [24].

$Q_{Tot} = \dot{m} \times [H_{He4}(P_{in}, \theta_{in}) - H_{He4}(P_{out}, \theta_{out})]$, based on the energy balance equation, θ_{out} is calculated as a function of Q_{Tot}, P_{in}, P_{out}, θ_{in}, and $\dot{m}$. The effective thermal resistance for the heat extraction by Helium from the superconductor (under normal operation) includes the following -

i. Flowing helium inside the SS tube (based on the Dittus-Boelter equation, eqn. 7),

$$h_{conv\_SS}(V_{cc}, D_{cc}, P, \theta) = K_{He}(P, \theta) \times \frac{Nu(V_{cc}, D_{cc}, P, \theta)}{D_{cc}} \quad .. (7)$$

Where,

$$Nu(V_{cc}, D_{cc}, P, \theta) = 0.023 \times Re(V_{cc}, D_{cc}, P, \theta)^{0.8} \times \Pr(P, \theta)^{0.4} \quad ..(8)$$

$$Re(V_{cc}, D_{cc}, P, \theta) = \frac{\rho_{He4}(P,\theta).V_{cc}.D_h(D_{cc})}{\mu_{He}(P,\theta)} \quad .. (9)$$

ii. Across the central perforated stainless steel tube thickness, and

iii. Across the static helium filled voids between the strands.

The overall heat transfer co-efficient is calculated using the three heat transfer co-efficient components based on an equivalent thermal resistance model as shown in Fig. 7 and subsequently defined for a unit length (eqn. 10-11),

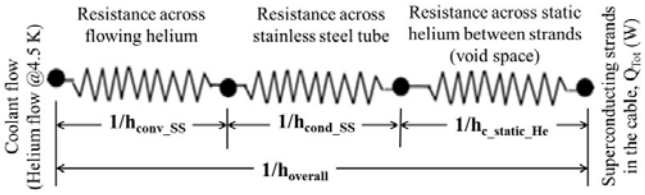

Fig. 7: An equivalent thermal resistance model showing the overall heat transfer resistance for extraction of heat from the superconductor by Helium

$$h_{overall\_UL}(V_{cc}, D_{cc}, P, \theta) = h_{overall}(V_{cc}, D_{cc}, P, \theta) \times \pi D_{cc} \quad .. (10)$$

Where,

$$h_{overall}(V_{cc}, D_{cc}, P, \theta) = \left[\left(h_{conv\_SS}(V_{cc}, D_{cc}, P, \theta)\right)^{-1} + \left(h_{c\_static\_He}(P, \theta)\right)^{-1} + \left(h_{cond\_SS}(\theta)\right)^{-1}\right]^{-1} \quad .. (11)$$

Summary of helium flow rates (with coolant pressure drops) required to limit the temperature rise, to no higher than 1 K, at varying ramp rates is provided in Table VI. The variations of the overall heat-transfer and temperature rise are shown in Fig 8 (a-b) for helium flow rates between 0.35 g/s to 2.0 g/s. The magnitude of the heat-transfer co-efficient tends to plateau at higher flow rates. Therefore, the present analysis has been limited to a flow-rate of 2.0 g/s. Analysis shows the temperature rise can be limited to 1 K at 1.0 T/s with 2.0 g/s at 2.5 bar inlet pressure. This suggests that the temperature rise can be managed with increased helium flow to a level before the heat transfer co-efficient plateaus and limits the heat extraction capability. The pressure drop is not insignificant but is manageable.

TABLE VI

SUMMARY OF HELIUM PARAMETERS VS RAMP-RATES

Series Cryogenic Cooling Circuit (85 m for both coils)			
Parameter	**1.0 T/s**	**0.5 T/s**	**0.25 T/s**
Helium flow rate (g/s)	2.0	2.0	2.0
Inlet Pressure of Helium (bar)	2.5	2.5	2.5
Helium pressure drop (bar)	0.71	0.71	0.71
Helium inlet temperature (K)	4.5	4.5	4.5
Max. conductor temperature (K)	5.434	5.013	4.919
Max. CICC temperature rise (K)	0.934	0.513	0.419

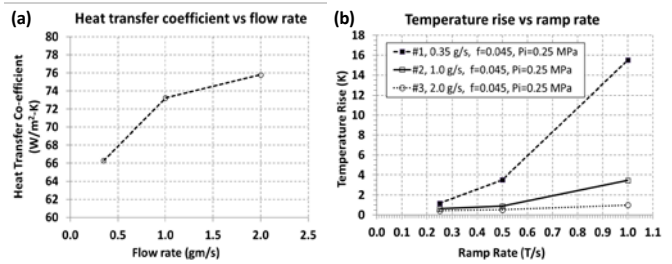

Fig. 8: (a) estimation of overall heat transfer co-efficient vs helium flowrate (b) estimation of the temperature rise with ramp rate

C. Model equivalent single coil quench analysis

The stored energy of the model 3 T-SF dipole is ~75 kJ and a dump resistor of 0.05 Ω is used to extract the energy externally. An equivalent single coil Wilson model [6] is used for a preliminary quench calculation.

Quench Integral: The quench integral or quench load, (also sometimes referred to as MIITs), is evaluated based on the Wilson Model [6] as indicated below (eqn. 12) for a worst case scenario in the event of a quench, where the current density remains constant at the initial value for the whole decay time. The MIITs calculation uses only the material properties of the conductor to evaluate the time required to reach a certain temperature. The user then has to use this information to establish the time interval to reach a 'safe' temperature for the weakest point in the magnet (for example the melting point of any solder used for making conductor joints).

$$\int J(t)^2 dt = \int_{4.7K}^{T_m} \frac{\gamma.C(T_{cond})}{\rho(T_{cond})} dT_{cond} \quad .. (12)$$

Two scenarios were investigated to evaluate the required magnet protection. Assumption, the quench would start from one spot and that spot gets continuously heated under adiabatic conditions. MIITs is evaluated both with dump resistor and without the dump resistor (all energy dumped in the coil).

- Case#1*:* Model dipole without any active quench heaters, with the whole conductor length active in each half of the dipole (42.5 m);
- Case#2: Model dipole with active quench heaters on one side of both top and bottom coils. Assuming an active conductor length of approximately 3.5 m each turn of one half

of the dipole as an effective length of conductor *(considering all turns are of equal length for the analysis*), as shown in Fig 3.

A resistive quench heater foil is located at one end of the body length of the dipole, as shown in Fig. 9. Each serpentine shaped quench heater foil is in thermal contact with each turn of the CICC for both the top and bottom coils (length of conductor evaluated is about 42.6 m/12 turns per dipole = 3.5 m). A summary of calculated critical parameters are presented in Table VII. Characteristic parameters like Minimum Quench Energy (MQE), Length of Minimum Propagation Zone (MPZ) have been calculated for future reference and will be required for the design of splices and coil interconnects/bus bars and overall magnet stability.

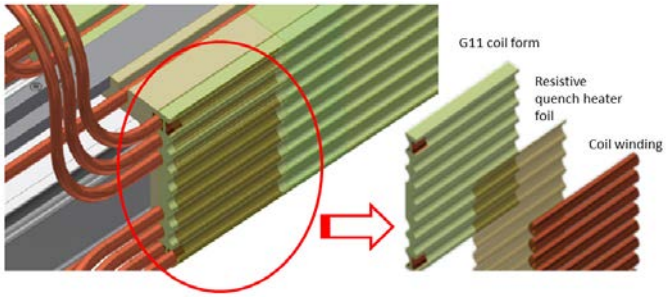

Fig. 9: Schematic representation of quench heater location and mounting

TABLE VII
BRIEF SUMMARY OF CALCULATED CRITICAL PARAMETERS

Parameter (calculated)		Case#1	Case#2
Operating temperature (K)		4.92	
Current sharing temperature (K)		6.97	
Temperature margin (K)		2.05	
Short sample performance (%)		61.9	
MPZ (mm)		0.16	
MQE (mJ)		3.79	
Conductor length used for quench calculation (m)		42.5	3.5
Hot spot temp. (K) / Time to reach the corresponding hot spot temperature (ms)	*Initial*	53.9/21.7	70.9/ 39.81
	Final	>2000†/781	140/65
Max. voltage, Line to Ground (kV)		> 2.5	1.3
Max. MIITs at 200 K (10^6.A^2.s)		-	16.2
MIITs estimated with dump resistor (10^6.A^2.s)		-	1.19
Time required to run the magnet to 0 A incl. detection time (ms) *for design*		-	< 49

†*unsafe leading to magnet damage*

Preliminary analysis for Case#1 (with conductor length 42.5 m in one-coil of the dipole) suggests that an excessive temperature rise will occur at the point of quench initiation (*also referred to as the hot spot temperature*), with potential damage to the coil. Case #2 suggests a hot spot temperature of ~140 K in 65 ms, with MIITs limited to ~ 16.2 MA^2s for a 200 K temperature rise without a dump resistor and 1.19 MA^2s with a dump resistor suggesting that the magnet should be safe. The quench heater foil (used in case #2) is assumed to be an ideal heater that can transfer the heat instantaneously to the conductor, therefore for future studies a thermal time constant will need to be added to the overall time. The analysis also suggests that the time required to run the magnet down (which includes the quench detection time), should be less than 49 ms which is an extremely challenging requirement. Therefore, fast active protection is one critical requirement using fast-electronics to sense and interrupt the current from the power supply to ensure the safety of the magnet.

D. Magnet stability

The model dipole was also evaluated for stability with the given conductor under static conditions at full operating current using multiple stability criteria [4], [25]-[26]. The summary of the stability evaluation is given below in Table VIII.

The short sample performance and the temperature margin suggest that magnet is stable but will require a tighter filament twist pitch for the overall magnet stability. One perceived benefit having CICC is having a direct contact between the superconducting strands and supercritical helium is envisaged to dissipate micro-quenches before they propagate [8].

TABLE VIII
SUMMARY OF SF MODEL DIPOLE STABILITY

Parameters evaluated	Passed	Remarks
Short sample performance (SSP) in %	Yes	< 75 (†62.8)
Temperature margin (Sharing temperature) K	Yes	>1.5 (†1.97)
Stable for Beta (Adiabatic stability)	Yes	
Adiabatic flux jump stability	Yes	
Dynamic stability	Yes	
Filament twist pitch stability	*No*	*need <7.15 mm*
Stable for finite element size	Yes	
Cryogenic Stability	*	*Not for the CICC*

†calculated values

IV. RISK MITIGATION APPROACH

At the present stage this design has been subjected to a Failure Modes and Effects Analysis (FMEA) process, limited to failure mitigation from a technical perspective, driving designs that will achieve safe operation of the magnet system based on the experience gained from the 12 GeV upgrade project at JLab [27]. The primary focus has been on the protection system and its adequacy for the proposed magnet design.

JLab utilized the FMEA methodology to identify the highest risk aspects of the CICC. This paper identifies the first series of analyses performed in response to the identified risks, via ranked Risk Priority Number (RPN). Due to the requirement that accelerator magnets exhibit design robustness, it is critical to fully validate the CICC design, refining as necessary, in order to be seen as equivalent in robustness to Rutherford cable.

The FMEA is applied using the RPN c*riteria* – potential failure modes, potential effects of failure, potential causes, and controls that could be in place with recommended actions. The RPN is evaluated based on the severity (S), occurrence (O) and detection (D) level/ranking, given in Tables IX, X and XI respectively. The following *entities* have presently been evaluated based on the RPN - splices, conductor, magnet, support structure, electrical failure, vacuum vessel and pumping system, control system, steel and beam-chamber during the preliminary design. A Detection Probability was generated based on the likelihood of mitigation before the issue became a failure or detection before it has a significant consequence. A RPN-After-Mitigation (RPN-AM) was generated from the

product of the three values S, O and D. A sample of the identified failure modes are presented in Table XII for the conductor and magnet. The Failure Modes were grouped into three levels by these RPNs: low risk <18, moderate risk <45 and high risk ≥45. FMEA exercise suggests that further studies, analyses, short sample testing, and prototype program are necessary to demonstrate the robustness for CICC and the magnet.

TABLE IX
LEVEL WITH RANKING OF SEVERITY

Value	Effect	Severity
1	No Impact	No impact to fit, form, or function.
2	Negligible	Potential for impact on appearance or an annoyance if a component, system, subsystem, or assembly does not meet design requirements.
3	Marginal	Potential for a moderate impact or loss of the secondary function of a component, system, subsystem, or assembly if it does not meet design requirements.
4	Significant	Potential for an adverse impact or degradation of primary function if a component, system, subsystem, or assembly does not meet design requirements.
5	Critical	Potential for serious impact or loss of primary function of a component, system, subsystem, or assembly if it does not meet design requirements.
6	Crisis	Potential for violation of a regulation or catastrophic failure during operation if the component, system, subsystem, or assembly does not meet design requirements

TABLE X:
LEVEL WITH RANKING AND PROBABILITY OF OCCURRENCE

Value	Effect	Occurrence Risk	Probability
1	Improbable	Few failures with identical design.	Occurring not more than once in its life time.
2	Remote	Few failures with similar design.	Occurring not more than once in ten years.
3	Occasional	Frequent failures of similar designs, or failure not likely with new design or application.	Occurring not more than once in five years.
4	Probable	Failures expected with new design or application.	Could occur once in two years.
5	Frequent	Failures inevitable or new design without precedent.	Could occur annually.

TABLE XI
LEVEL WITH RANKING AND PROBABILITY OF DETECTION

Value	**Detection** Likelihood	**Detection** (Design Controls)	**Detection** (Operational Design Controls)
1	Almost Certain	Failure prevented through proven design solution.	Failure mode almost certainly detected by continuous automatic online testing.
2	High	Analysis with strong detection capability and high correlation to operating conditions.	Failure mode likely detected by continuous automatic online testing.
3	Medium	Product validation testing prior to design freeze.	Failure mode likely detected by periodic online testing/monitoring.
4	Low	Product validation testing prior to launch, but after design freeze.	Failure mode likely detected by periodic offline testing or inspection.
5	Very Low	Analysis with weak detection capability or low correlation to expected operating conditions.	Failure mode only likely to be detected by unplanned testing or inspection.
6	Remote	No design controls in place.	Failure mode not detectable in service.

V. CONCLUSIONS AND OUTLOOK

In order to establish the performance with the new conductor, and to provide guidelines for testing, preliminary analyses of the 3T-SF model dipole have been carried out in order to set limits for the key operational parameters (cryogenics and electromagnetic) in terms of magnet stability during a fast ramp. The analyses have demonstrated a few limitations with the superconducting strands (in terms of instability), with filament twist pitch and impact on cryogenics (helium flow rate) for a fast ramping magnet (1 T/s). The AC losses can be reduced significantly and the effect can be mitigated with a tighter twist pitch and sizing of filaments together with proper selection of matrix material with improved thermal capacity. This will also help on the development of fast active protection to bring the magnet current down without damaging the magnet. It is critical to further identify the risks and have a full program of refining the Design for FMEA (DFMEA) with a complementary design validation, including testing of the CICC as well as full scale magnets.

TABLE XII
EXTRACT FROM THE FMEA WORKSHEET FOR THE FAST RAMPING 3 T SUPER-FERRIC BOOSTER MAGNET

FMEA WORKSHEET - Failure Mode & Effects Analysis										
Potential Failure Mode	**Potential Effects of Failure**	**S**	**Potential Causes**	**O**	**D (BM)**	**RPN-BM**	**Controls could be in place**	**D**	**Recommended Actions**	**RPN-AM**
Conductor: Design (Structural, Pressure)	Conductor overpressure and burst	6	Overpressure during quench event	4	3	**72**	Adequate design analysis and safety design with reliefs as per ASME and JLab standard	1	Adequate design to accommodate the quench scenario with all energy dumped in the conductor	**24**
Conductor: AC losses for fast ramping magnets	Increased Heat load on the conductor and magnet during ramping	4	Filament size and twist pitch of Sc filament with the Base material matrix of the strands	3	3	**36**	Appropriate design analysis carried out using published data	1	Appropriate selection of conductor with proper filament size and twist pitch	**12**
Conductor: Stability	Increased Heat load and hot spot temperature during ramping and quench	6	Not enough thermal stabilizer and improper design (magnet, buslead, splice), burnout	4	2	**48**	Adequate design analysis and reviews (design stage)	1	Adequate design to accommodate the quench scenario	**24**

Conductor: Cooling mechanism inadequate	Conductor at elevated temperature	5	Limited flow, high heat load, high ac losses during ramping, yoke at elevated temperature	4	3	**60**	develop the operating boundary and predict with FEA & analytical models	1	Adequate selection of Flow, pressure and controlled ramp	**20**
Conductor: Burn out of the conductor in case of a quench	Inadequate cooling and hot spot temperature too high to handle and propagate	5	inadequate design of the magnet and protection circuit	4	4	**80**	Adequate protection design analysis (design stage)	1	Design and test to define- a reference or adopt any reference design used in the past	**20**
Magnet: Could not make 1 T/s	Effect the performance of the magnet requirement	4	Inadequate conductor, cooling capacity and heat load, others	4	4	**64**	Design and test R&D prior to actual magnet design and built for the system	2	Design and test to define the boundary condition	**32**
Magnet: Coil cannot accommodate high flow rates	Reduced cooling and reduced temperature margin	4	Cryogenic limitation and block in the cooling path/high heat load	4	3	**48**	develop the operating boundary and predict with FEA & analytical models	1	Adequate selection of Flow, pressure and controlled ramp (determine the ramp rate envelope)	**16**

SEVERITY (S) = How severe is effect on the customer; OCCURANCE (O) = How often or frequent; DETECTION (D) = How probable is detection of cause; RPN = S * O * D; RPN-BM is RPN before mitigation; RPN-AM is RPN after mitigation; D (BM) = Detection (before mitigation); Maximum RPN = 6 (S) * 5 (O) * 6 (D) = 180.

ACKNOWLEDGEMENTS

The work reported here is a result of very close teamwork between the design groups at the Accelerator Research Lab and Jefferson Lab. Authored by Jefferson Science Associates, LLC under U.S. DOE Contract No. DE-AC05-06OR23177. The U.S. Government retains a non-exclusive, paid-up, irrevocable, world-wide license to publish or reproduce this manuscript for U.S. Government purposes.

REFERENCES

[1] T. Satogata, Y. Zhang, "JLEIC-A Polarized Electron-Ion Collider at Jefferson Lab, JLEIC Design study Collaboration," ICFA-*Beam Dynamics Newsletter*, No.74, p92, Aug. 2018

[2] A. Accardi, *et al.* "Electron-Ion Collider: The Next QCD frontier Understanding the glue that binds us all", *Eur. Phys. J.* A52 (2016) no.9, 268, DOI: 10.1140/epja/i2016-16268-9.

[3] P. McIntyre *et al.*, 'Cable-in-Conduit Dipoles for the Ion Ring of JLEIC', *IEEE Trans. Appl. Supercond.*, V29 (5), 2019, 4004806.

[4] M. N. Wilson, "Superconducting magnets," *Oxford University Press*, UK, 1983, pp158-198.

[5] M. Wilson, "NbTi Superconductors with Low AC Loss: A Review", *Cryogenics*, V48, Issues 7-8, pp381-395, 2008

[6] M. N. Wilson, "Superconducting magnets," *Oxford University Press*, UK, 1983, pp151-231.

[7] Peter McIntyre, *et al.*, "Quench protected structured superconducting cable," US Patent US20160049225A1, Feb. 2016

[8] A. D. Kovalenko, "Cable design and related issues in a fast-cycling superconducting magnets," *IAEA-INIS, Proceedings Workshop on accelerator magnet superconductors, France*, INIS-FR-5606, V38 (17), 38041657, 2004

[9] J. Kaugerts, et *al.*, "Cable design for FAIR SIS-300," *IEEE Trans. Appl. Supercond.*, V17 (2), June 2007, DOI 10.1109/TASC.2007.898474

[10] G. A. Kirby, *et al.*, "Fast ramping superconducting magnet design issues for future injector upgrades at CERN," *IEEE Trans. Appl. Supercond.*, V18 (2), 2008.

[11] J. Kaugerts, *et al.*, "Cable design for FAIR SIS 300", *IEEE Trans. Appl. Supercond.*, V17 (2), 2007.

[12] L. Bottura, "A Practical Fit for the Critical Surface of NbTi", *IEEE Trans. Appl. Supercond.*, V10 (1), pp.1054-1057, March 2000, DOI: 10.1109/77.828413

[13] M. N. Wilson, *et al.*, "Design studies of superconducting Cos θ magnets for a fast pulsed synchrotron," *IEEE Trans. Appl. Supercond.*, V12 (1), March 2002.

[14] P. Fabbricatore, *et al.*, "Rapid cycling superconducting magnets," *Elsevier Publications - Nuclear Physics B (Proc. Suppl.)*, 154, p157, 2006, DOI: 10.1016/j.nuclphysbps.2006.01.051

[15] P. Bruzzone, A. Nijhuis, and H. H. J. ten Kate, "Effect of Cr plating on the coupling current loss in cable-in-conduit conductors," in *ICEC-ICMC-96*, p1243.

[16] L. Tkachenko, *et al.*, "Development of a superconducting dipole with Fast-cycling magnetic field", *Proc. of EPAC*, Paris, France, pp2436-2438, 2002

[17] G. Moritz, "Fast-Pulsed Sc Magnets," *Proc. of EPAC*, Lucerne, Switzerland, 2004.

[18] Y. Wachi, M. Ono, T. Hamajima, "Heat transfer characteristics of the supercritical helium in a cable-in-conduit conductor", *IEEE Trans. Appl. Supercond.*, V5 (2), p568, 1995

[19] L. Bottura, "Thermohydraulics of CICC's with central cooling passage", *IEEE Trans. Appl. Supercond.*, V5 (2), p745, 1995

[20] N. Martovetsky, *et al.*, "Effect of conduit material on CICC performance under high cycling loads", *IEEE Trans. Appl. Supercond.*, V15 (2), p1367, 2005

[21] D. Chavez, "Design and development of Cable-in-Conduit superconductor technology for the magnets of the Future Electron-Ion Collider," *PhD Dissertation*, Universidad de Guanajuato, Leon, Guanajuato, Mexico (*January 2018*).

[22] R. Zanino, P. Bruzzone, L. S. Richard, "A Critical Assessment of press Drop Design Criteria for the Conductor of ITER Magnet" *CP823, Advances in Cryo Eng.: Transactions of the Cryogenic Engg. Conf. – CEC*, V51, p1765, 2006.

[23] B. J. McKeon, A. J. Smits, "Static pressure correction in high Reynolds number fully-developed turbulent pipe flow, *Meas. Sci. Technol*., 14, pp1608–1614, 2002.

[24] V. D. Arp, R. D. McCarty, D. G. Friend, "Thermophysical Properties of Helium-4 from 0.8 to 1500 K with Pressures to 2000 MPa", *NIST Technical Note 1334 (Revised)*, National Institute of Standards and Technology (NIST), U.S. Government Printing Office, USA, September 1998

[25] V. E. Sytnikov, *et al.*, "Development and Test of a Miniature Novel Cable-In-Conduit-Conductor for Use in Fast Ramping Accelerators With Superconducting Magnets," *IEEE Trans. Appl. Supercond.*, V16 (2), June 2006, DOI: 10.1109/TASC.2006.873237

[26] N. Martovetsky, "Stability and thermal equilibrium in cable-in-conduit conductors," *Physica C: Supercond.* V 401, pp118–123, 2004.

[27] P. Ghoshal, *et al.*, "FMEA on the Superconducting Torus for the Jefferson Lab 12 GeV Accelerator Upgrade," *IEEE Trans. Appl. Supercond.*, V25 (3), Jun. 2015, 4901005, DOI: 10.1109/TASC.2015. 2388591

Probir K. Ghoshal (M'05–SM'11) received the B.E. (Hons.) degree in electrical engineering from the Government Engineering College, Bilaspur, India, in 1992, the M.Tech. degree in cryogenic engineering from the Indian Institute of Technology, Kharagpur, India, in 1995, and the Ph.D. degree in electrical engineering from the University of Cambridge, Cambridge, U.K., in 2009.

From February 1995 to Dec 2000, he was a Project Engineer/Assistant Manager with engineering and cryogenic industry. From January 2001 to December 2010, he worked for Oxford Instruments NanoScience involved with various superconducting magnets including world's highest fully superconducting magnet 22.5 T using both LTS and HTS as a Principal Engineer. He

moved to the USA working for General Electric—Global Research Center, Niskayuna, NY, USA, from December 2010 to January 2013 on applied superconductivity and cryogenics. Since January 2013, he has been working as a Senior Staff Engineer (Supercon-ducting Magnet Engineer) with the Magnet Group within Experimental Nuclear Physics, Thomas Jefferson National Accelerator Facility, Newport News, VA, USA. He also contributed a chapter to High Temperature Superconductors (HTS) for Energy Applications (Cambridge, U.K.: Woodhead Publishing Ltd., 2011). He has publications in review journals and patents.

Dr. Ghoshal is a Technical Editor and Reviewer for the IEEE TRANSACTIONS ON APPLIED SUPERCONDUCTIVITY and a Reviewer for Superconducting Science and Technology (Institute of Physics, U.K.). He is a Chartered Engineer, a Member of the Institute of Engineering and Technology (U.K.), a Member of Indian Cryogenic Council, and a Member of Indian Vacuum Society.

Daniel Chavez received the B.S. (Physics) from the Universidad Autonoma de Zacatecas, Zacatecas, Mexico in 2012, and the M.Sc. (*Laurate*) and Ph.D. (*summa cum laude*) in Physics from Universidad de Guanajuato, Leon, Guanajuato, Mexico in 2015 and 2019 respectively.

In 2014, he joined the Accelerator Research Laboratory at the Texas A&M University, at College Station, Texas as a research assistant. Later in 2019, he joined the Accelerator Technology Corp (R&D Division), College Station, TX, USA as staff Scientist in charge of developing Cable-in-conduit technology for large-scale applications.

Dr. Chavez is a member of the American Physics Society, a founder member of the Mexican Particle Accelerator Community, and a Member of the High-energy physics network in Mexico. Dr. Chavez won first position in the Applied Superconductivity Conference (Seattle 2018), student competition in the large-scale application of superconductors.

Ruben J. Fair (SM'11) received the B.Sc. (Hons.) Eng. degree in electrical engineering and the Ph.D. degree in electrical engineering from the Imperial College of Science and Technology, London, U.K., in 1985 and 1991, respectively.

In 1988, he joined GEC-Alsthom Large Machines, Ltd., as a Hydrogenerator Design Engineer and left in 1994 to join Oxford Instruments (NMR division) as a Design and Development Engineer working on a range of new superconducting magnets, including the world's first persistent 900-MHz NMR magnet. In 1999, he became a Principal Engineer at Oxford Instruments (Research Instruments) to lead a team of engineers developing superconducting magnets and ultralow temperature refrigerators for the physics community. In 2005, he was selected to lead the new product introduction engineering team, Oxford Instruments Nanoscience. In 2007, he joins Converteam (now General Electric Power Conversion) where he led a team of engineers to develop the world's first high temperature superconducting hydrogenerator and also set up a Cryogenics Laboratory. In 2010, he was recruited by the General Electric Global Research Center, Niskayuna, NY, USA, to develop a strategic road map for a range of superconducting machines. While at the research center, he led a team which was awarded funding from the Department of Energy to design a superconducting wind turbine generator. He accepted a position as a Principal Engineer at the Jefferson Laboratory, Newport News, VA, USA, in 2013 to lead a team overseeing the design, build, installation, and commissioning of eight superconducting magnets for the 12 GeV accelerator upgrade project. He also contributed a chapter to High Temperature Superconductors (HTS) for Energy Applications (Woodhead Publishing, 2011). He has publications in review journals and patents.

Dr. Fair is a Technical Editor and Reviewer for the IEEE TRANSACTIONS ON APPLIED SUPERCONDUCTIVITY. He is a Chartered Engineer and a Member of the Institute of Engineering and Technology, U.K.

Sandesh Gopinath completed his B.E in mechanical engineering from K. J. Somaiya College of Engineer, Mumbai, India, in 2011, and the M.S. degree in mechanical engineering from Rutgers University, New Jersey, USA, in 2015.

From 2012 to 2015, he worked as a graduate research assistant in the Mazzeo Research Group at Rutgers University, New Jersey with emphasis on electroacoustic. Since 2016, he started working with Jefferson Lab (JLab), Newport News, VA, USA. He primarily contributed to design and built of vacuum-based high temperature material testing apparatus for experimental nuclear physics. Since 2018, he has been working as a Staff Engineer in Magnet Group within experimental nuclear physics at JLab where he contributes towards development of accelerator and detector magnet system utilizing multi-physics simulations.

David H. Kashy received the B.E. degree in mechanical engineering from Michigan State University, East Lansing, MI, USA, in 1982 and the M.E. degree from Old Dominion University, Norfolk, VA, USA, in 1997.

In 1983, he started his professional career with Ing. Technical Department, Newport News Shipbuilding, as a Mechanical Engineer. In 1988, he joined Cryogenics Department, CEBAF, as a Mechanical Engineer. In this position, he designed the cryogenic hardware including helium purifiers, distribution valve boxes, and transfer lines and helped with commissioning several large-scale refrigerators including the 4.8 kW and 2 K refrigerator. Later became a Lead Engineer for Experimental Hall B where he led a group of engineers, designers, and technicians in designing hardware for the experimental physics program along with maintenance and operation of this hardware, which included a large superconducting toroidal magnet along with smaller magnets and cryogenic targets. In 2012, he was a Lead Engineer to design, build, install, and commission a new toroidal magnet, the CLAS12 Superconducting Torus. Since November 2017, he has been working as a Senior Staff Engineer (Mechanical Engineer) with the Magnet Group within Experimental Nuclear Physics, Thomas Jefferson National Accelerator Facility, VA, USA. He has publications in review journals.

Mr. Kashy became a licensed PE in 1988 in the state of Virginia, USA.

Peter McIntyre…

Timothy Michalski received a B.S. degree in mechanical engineering from Rochester Institute of Technology, Rochester, NY, USA, in 1988 and the M.S. degree in engineering management from Syracuse University, Syracuse, NY, USA, in 2002.

In 1988, he started his professional career with Harris Corporation, RF Communications Division, as a Mechanical Engineer in the development and testing of strategic and tactical HF/VHF/UHF radio equipment. In 1998, he joined Philips Broadband Networks, as a Mechanical Project Engineer and Engineering Manager developing CATV distribution and headend equipment. In 2003, he joined BorgWarner Morse-TEC as a Project Engineer and Engineering Manager, developing engine timing drives for US and international automobile manufacturers. In 2004, he joined PAR Technologies LLC (which later became AdaptivEnergy LLC) as a Project Engineer and Engineering Manager in the development of Ruggedized Laminated Piezo (RLP) devices for a variety of industrial application. While there, he also assumed the role of VP of Engineering and ultimately VP/General Manager. In 2010, he joined Thomas Jefferson National Accelerator Facility as the Engineering Division Deputy. In this role, he manages several groups and drives the engineering product development process. He also has been Engineering Project Lead for the g2p beamline upgrade in experimental hall A, the high power beam dump upgrades in experimental halls A and C, and the development of the Jefferson Lab Electron-Ion Collider (JLEIC).

Renuka Rajput-Ghoshal (M'19) received the B.Sc. & M.Sc. (Physics) degree from the Rohilkhand University, Bareilly, India, in 1985 and 1987 respectively, and the Ph.D. degree in physics from the Jawaharlal Nehru University, New Delhi, India in 1993.

In 1992, she joined National Physical Laboratory, New Delhi as a Research Associate to design India's first NMR magnet. In 1994 she joined Raja Ramanna Centre for Advanced Technology (RRCAT, formerly known as CAT), Department of Atomic Energy of India as Scientific Officer. From August 2001 to May 2004, she worked for Oxford Instruments, Eynsham, UK with various superconducting NMR magnets. In June 2004, she joined Scientific Magnetics (formerly known as Space Cryomagnetics Ltd.), Abingdon in the UK as a senior magnet engineer/physicist. She lead the design and analysis of various superconducting magnets for physical sciences, vector rotate magnets, AMS magnet (world's first magnet planned to go in space), and research magnet for particle detectors. She moved to the USA working for General Electric—Global Research Center, Niskayuna, NY, USA, from January 2011 to January 2013 on applied superconductivity and cryogenics. Since February 2013, she has been working as a Senior Staff Engineer (Superconducting Magnet Engineer) with the Magnet Group within Experimental Nuclear Physics, Jefferson Laboratory, Newport News, VA, USA. She has publications in review journals and patents.

Dr. Rajput-Ghoshal is a Technical Editor and Reviewer for the IEEE

TRANSACTIONS ON APPLIED SUPERCONDUCTIVITY and a Reviewer for Superconducting Science and Technology (Institute of Physics, U.K.). She is a Chartered Physicist and a Member of Institute of Physics, UK, a Member of the American Physical Society (USA.), and a Member of Indian Cryogenic Council.

Akhdiyor Sattarov received the M.Sc. (applied mathematics) degree from Sankt Petersburg State University, Sankt Petersburg, Russia in 1987 and the Ph.D. degree in physics and mathematics from Institute of Nuclear Physics, Tashkent, Uzbekistan in 1998.
In 1998, he joined Accelerator Research Laboratory of Dept. of Physics and Astronomy, Texas A&M University as a Post-Doctoral Research Associate. There he became Associate Research Scientist in 2002 and Research Scientist in 2011. He led the design and analysis superconducting accelerator magnets, magnets for MR spectroscopy, RF-cavities, beam dynamics in accelerators, nuclear fuel dynamics in accelerator driven systems. Since June 2018, he is a Research Scientist at Accelerator Technology Corp., College Station, TX, USA and working on high field dipoles based on superconducting cable in conduit. He has publications in peer-reviewed journals and 3 patents.